Nanoscale Advances

ROYAL SOCIETY OF CHEMISTRY

COMMUNICATION

View Article Online
View Journal | View Issue

Cite this: *Nanoscale Adv.*, 2022, **4**, 2988

Received 22nd February 2022
Accepted 31st May 2022

DOI: 10.1039/d2na00123c

rsc.li/nanoscale-advances

Higher-order assembly of BSA gold nanoclusters using supramolecular host–guest chemistry: a 40% absolute fluorescence quantum yield†

Anjan Maity *[a] and Atul Kumar[b]

Herein, we report for the first time a highly emissive higher-order assembled structure of BSA-Au NCs in the presence of cucurbit[7]uril, which enhances the absolute fluorescence quantum yield of BSA-Au NCs up to 40%. Cucurbit[7]uril neutralizes the surface charge of BSA-Au NCs, and hence aggregation happens. This aggregation shows reversible disaggregation in the presence of adamantylamine.

Noble metal nanoclusters (NMNCs) are emerging functional nanomaterials.[1] The photophysical properties of NMNCs were found to be influenced by their intrinsic structure, composition, and core size, and the environment around NCs, including solvent and protecting ligands.[2–4] The functional properties of NMNCs can be easily tuned by using different ancillary ligands such as thiolates,[5] phosphine,[6] alkyne,[7] *etc.* Although light-emissive NCs are in high demand due to their optoelectronic properties, the emergence of luminescence behavior in NCs has not been fully elucidated. However, some studies reveal the role of ligand-to-metal charge transfer (LMCT)[8] and/or ligand-to-metal–metal charge transfer (LMMCT)[9] in designing emissive NCs. The nature of ligands in the cluster plays a pivotal role in surface functionalization and hence opens the opportunity to tune the fluorescence quantum yield (QY) of NCs. Current research focuses on small-molecule-protected NCs for practical applications,[10] but the lack of biocompatibility restricts their use in biology. In this context, protein-protected noble metal nanoclusters (PPNMNCs) found their widespread use in various applications such as biomedical imaging,[11] sensing,[12] and so forth. Biocompatible luminescent PPNMNCs would be ideal if they exhibited a high quantum yield. However, because of their low quantum yield,[13] their real applications such as cell imaging are hampered. So, the design of highly fluorescent PPNMNCs remains a challenging task for synthetic and materials scientists. To design such complex molecular architectures, synthetic chemists utilize supramolecular approaches to generate superstructures of nanomaterials by the assembly of simple molecules *via* noncovalent interactions such as hydrogen bonding interactions, π–π interactions, hydrophobic interactions, and van der Waals (vdWs) interactions.[14,15] Molecular cages like cucurbit[7]uril (CB7) and cyclodextrins (CDs) possess a hydrophobic cavity and hence *via* molecular encapsulation/host–guest interactions they can form large assembled superstructures. Recently, attempts have been made through the supramolecular host–guest complexation of $Ag_{29}LA_{12}$ with CB7 and β-CD to enhance the luminescence properties.[16] Supramolecular host–guest interactions can also provide remarkable improvement in stability and concomitant enhancement in the properties of the gold NCs of $[Au_{25}(SBB)_{18}]$ with β-CD.[17] Metal ions-induced is another method to enhance the luminescence of protein-protected gold nanoclusters.[18] Aggregation-enhanced emission (AEE) is an intriguing optical phenomenon in which the weakly luminescent nanocluster displays remarkably enhanced emission in its aggregate state.[19] According to the literature, the supramolecular assembly can also alter the optoelectronic properties of colloidal nanoparticle clusters.[20] To the best of our knowledge, there is no report on cage compounds, such as CB7 and β-CD, for the fluorescence enhancement of protein-protected NCs through supramolecular host–guest chemistry. So, taking into account supramolecular chemistry, we introduce a noble technique to enhance the fluorescence by supramolecular host–guest chemistry in PPNMNCs. Towards this end, we report a host–guest driven higher-ordered assembled system of BSA-Au NCs in the presence of CB7. The encapsulation of amino acids inside the cavity of CB7 drives its emission enhancement, where we observe the absolute fluorescence quantum yield to reach up to 40.56%. We also observe that CB7 reduces the surface charge of PPNMNCs, and hence aggregation happens. Furthermore, in the presence of adamantylamine (ADA), the turbid system (assembled system) turns into a clear solution showing the reversibility of

[a]*Materials Research Centre, Indian Institute of Science, Bangalore, 560012, India. E-mail: anjanchem93@gmail.com; anjanmaity@iisc.ac.in*

[b]*Department of Inorganic and Physical Chemistry, Indian Institute of Science, Bangalore, 560012, India*

† Electronic supplementary information (ESI) available. See https://doi.org/10.1039/d2na00123c

protein-protected gold nanoclusters which is one of the fundamental aspects of protein aggregation which is generally irreversible in nature.[21] A schematic representation is demonstrated below for this system (Fig. 1).

To create a higher-order assembled structure, we have synthesized BSA-Au NCs and CB7.[22,23] In the solution, BSA forms an Au^{1+}-BSA intermediate and is finally converted into Au^{0}-BSA (in Au-BSA NCs) in the presence of NaOH. Here, BSA acts as a reducing agent as well as a stable capping agent for the gold nanocluster in an alkaline medium. BSA-Au NCs have been characterized using standard spectroscopic and microscopic techniques. The optical photograph of BSA-Au NCs in comparison with BSA suggests their formation (Fig. S1a–d†). A quantitative comparison of UV-vis spectra between BSA and BSA-Au NCs was performed to decipher their optical properties (Fig. S1e†). A distinct absorption peak at 280 nm was observed for both systems due to the presence of tyrosine and tryptophan in BSA. In addition to this, only BSA-Au NCs exhibit a shoulder hump from 350 nm to 450 nm. The absence of any well-defined absorption peaks in this region of BSA-Au NC confirms the presence of clusters inside BSA.[24] When BSA-Au NCs were excited at 365 nm, two emission maxima at around 450 nm and 645 nm were observed and assigned to weak protein emission and nanocluster emission, respectively (Fig. S1f†). The core size of NCs was measured and found to be below 2 nm by High-Resolution Transmission Electron Microscopy (HRTEM) analysis (Fig. S1g†). Additionally, the core size of NCs in terms of the number of gold atoms was further confirmed by MALDI-TOF Mass Spectrometry (MS) analysis (Fig. S2†). The protein shows a peak at $m/z \sim 66\,300$ while BSA-Au NCs exhibit a peak at $m/z \sim 70\,969$ with a mass difference of ~5 kDa. This mass difference is attributed to the formation of Au_{25}@BSA NCs. The molecular host CB7 has been synthesized, and characterization has been done by ^{1}H-NMR spectroscopy (Fig. S3†) and LC-MS (Fig. S4†). With this prior knowledge, the interaction of BSA-Au NCs with CB7 has been discussed in the next section.

Supramolecular cage CB7 encapsulates amino acids where they bind to its cavity *via* hydrophobic and electrostatic interactions.[25] The confinement of amino acids inside the cavity of CB7 restricts its rotational and vibrational motion and hence alters the luminescence behavior of BSA-Au NCs through aggregation-enhanced emission (AEE).[26] When we increased the concentration of CB7 up to 8 mM (CB7 in 5 mM PB buffer) in BSA-Au NCs, the appearance of turbidity within the system was noticed, and also, we observed a gradual increase in fluorescence intensity (Fig. 2a and b). The turbid mixture of BSA-Au NC@CB7 has been characterized using a confocal fluorescence image which suggests the formation of higher-order assemblies (Fig. 2c). The formation of higher-order assemblies was further confirmed by AFM images (Fig. S5†). Material characterization of the turbid system by HRTEM analysis clearly reveals the formation of a distinct assembled structure at the nanoscale (Fig. 2d). The formation of turbidity within the system was also analyzed *via* a turbidity measurement experiment of BSA-Au NCs in the presence of CB7 at 550 nm (Fig. 2e). Increasing the ratio of CB7/NCs leads to an increase in the scattering, and consequently, higher turbidity has been recorded at CB7/NCs ~ 125. This sudden jump of turbidity can be considered as an inflection point and called a critical assembled concentration. However, the turbidity gets saturated when the ratio of CB7/NCs is ~300. To investigate the effect of CB7 on the size of BSA-Au NCs, DLS measurements were performed. From the DLS study, we observed a gradual increase of the hydrodynamic size upon increasing the ratio of CB7 to BSA-Au NCs, and at the highest ratio, the size reached ~340 nm (Fig. 2f). We also characterized other non-turbid systems by confocal microscopy, which suggests the lack of formation of any higher-order assembly at a lower ratio of CB7 to BSA-Au NCs (Fig. S6–S10†). For fluorescence measurements, the concentration of CB7 varies from nanomolar to millimolar with respect to fixed protein concentration (Fig. S11†). We observed an ~3-fold increase in the emission intensity of BSA-Au NCs (Fig. 3a), which further increased to ~4.5-fold when a time-dependent fluorescence study was performed after 24 h (Fig S12†). In addition to emission enhancement, a blue shift of 10 nm was observed at

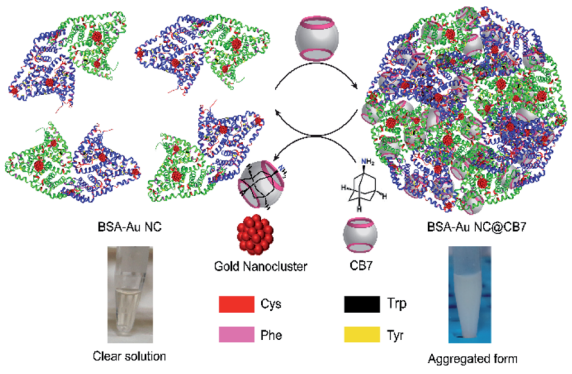

Fig. 1 Schematic representation of the formation of a higher-order assembled structure of BSA-Au NCs and its reversibility in the presence of ADA.

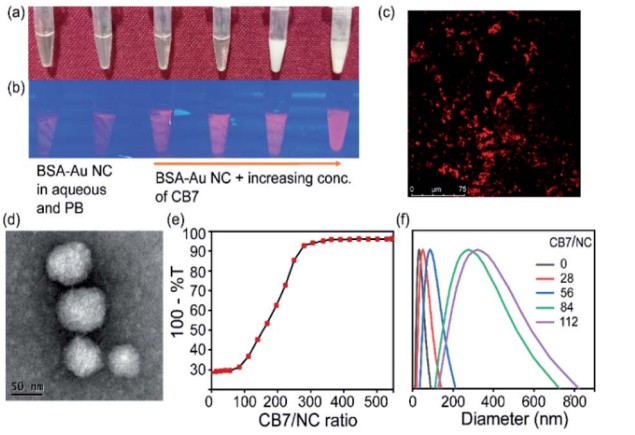

Fig. 2 Optical photographs of (a) BSA-Au NC@CB7 under visible light and (b) BSA-Au NC@CB7 under UV light. (c) A confocal fluorescence image of BSA-Au NC@CB7. (d) TEM image of BSA-Au NCs upon addition of CB7. (e) Turbidity measurement of BSA-Au NCs at different ratios with CB7 at 550 nm. (f) DLS measurement of BSA-Au NCs at different ratios of CB7 to BSA-Au NCs.

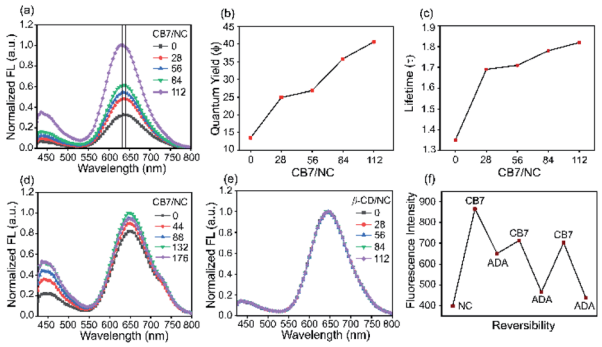

Fig. 3 (a) A normalized fluorescence emission spectra of BSA-Au NCs in the presence of CB7 (CB7 in 5 mM PB) (Ex. 365 nm). (b) A plot of the absolute fluorescence quantum yield of BSA-Au NCs at different ratios of CB7 and (c) a plot of fluorescence lifetime (τ in μs) of BSA-Au NCs at different ratios of CB7 to BSA-Au NCs. (d) A normalized fluorescence emission spectra of Lys-Au NCs in the presence of CB7 (Ex. 365 nm). (e) A normalized fluorescence emission spectra of BSA-Au NCs in the presence of β-CD (Ex. 365 nm). (f) A fluorescence reversibility plot of BSA-Au NCs upon simultaneous addition of CB7 and ADA.

the highest ratio of CB7 to BSA-Au NCs ~ 112 compared to CB7 to BSA-Au NCs ~ 28. This change in the emission profile in the presence of CB7 in BSA-Au NCs indicates amino acid encapsulation inside the cavity of CB7 (Fig. S13†).[27] At the highest concentration of CB7, we observed the formation of denser aggregates, which show emission at 645 nm when excited at 365 and 375 nm, respectively. The appearance of this same emission peak of BSA-Au NC@CB7 after the excitation at different wavelengths clearly suggests that the emergence of emission is not due to scattering but because of aggregation (Fig. S14†).[28] Also, increasing the concentration of CB7 with respect to BSA-Au NCs leads to an increase in absorbance at 230 nm and 280 nm (Fig. S15†). This UV-visible study clearly demonstrates the interaction between the amino acids of the protein shell of the nanocluster and CB7, which is also supported by fluorescence studies. The formation of higher-order assemblies is due to the aggregate formation, which in turn also increases the fluorescence intensity due to the AEE phenomenon. The AEE behavior was well supported by the quantum yield (ϕ_F) and lifetime (τ) measurements (Table 1, ESI†). A dilute solution of the cluster shows an absolute fluorescence quantum yield (ϕ_F) of 13.45%, but upon the addition of CB7, it reaches up to 40.56% (Fig. 3b and S16–S20†). With the increase in the ratio of CB7 to the BSA-Au NC, there is a gradual increase in the lifetime of BSA-Au NCs ($\tau = 1.35$ μs) to the assembled system ($\tau = 1.82$ μs) (Fig. 3c and S21†). To investigate the role of aggregation in energy transfer *via* FRET from Trp to the CB7 conjugated protein nanocluster, we excited the BSA protein, BSA-Au NCs, and BSA-Au NC@CB7 at 295 nm. Emission spectra show that there is a considerable reduction of fluorescence intensity at 340 nm from protein to the protein-protected nanocluster, indicating FRET from Trp to protein (Fig. S22†).[29] Further, an increase of the fluorescence intensity of both the protein and nanocluster was observed upon increasing the concentration of CB7, suggesting the absence of FRET from Trp to the cucurbit[7]uril conjugated BSA-Au NC. This result clearly suggests that FRET does not cause higher fluorescence quantum yield in the higher-order assembled structure. We have extended our observation to the lysozyme gold nanocluster to generalize our hypothesis. We synthesized the Lys-Au NC according to the literature procedure (Fig. S23†).[30] We got ~1.2 fold emission enhancement at the ratio of CB7 to Lys-Au NC ~ 132, but quenching happens at the highest ratio of ~176 (Fig. 3d). To investigate the role of the cavity dimension, we performed a fluorescence study with another host of β-CD (β-CD possesses a similar cavity dimension compared to CB7). However, the addition of β-CD does not alter its emission behavior, which suggests the absence of any interaction between the β-CD and BSA-Au NCs (Fig. 3e). This result proves that the host–guest interaction of CB7 with BSA-Au NCs is quite likely the electrostatic interaction between the negatively polarized carbonyl end of CB7 and the amino acids present in the BSA-Au NC.[31] We continued pH-dependent turbidity measurements where we observed a gradual enhancement of aggregation, and it got saturated in the acidic medium which suggests that the protonation of amino acids and electrostatic interactions play the major role in aggregation (Fig. S24†).[32] This hypothesis was further validated by zeta potential measurements, which showed a gradual decrease of the zeta-potential value from BSA-Au NCs to the cucurbit[7]uril conjugated BSA-Au NC system (Fig. S25 and Table 2, ESI†), but the CB7-conjugated BSA-Au NC system still possesses a negative charge on the surface. On the other hand, in the presence of CB7, Lys-Au NCs exhibit a positive surface charge (Fig. S25 and Table 3, ESI†). These studies prove that there is a surface charge neutralization process is taking place in PPNMNCs in the presence of CB7, and an increase in the hydrophobicity of the protein surface is responsible for higher-order assembly formation and causes aggregation. The higher quantum yield and lifetime are due to the AEE phenomenon; basically the electrostatic interaction between the carbonyl groups of CB7 and amino acids of the protein causes aggregation, and hence it rigidifies the whole assembled system. This rigidification promotes the radiative path and suppresses the non-radiative path.[26] It is worth mentioning that this phenomenon is fairly similar to aggregation-induced emission (AIE) where luminescence enhancement can be achieved through the restricted rotation of parts of luminophores.[33]

Protein aggregation is a fundamental problem in different kinds of neurodegenerative diseases such as Alzheimer's disease, Parkinson's disease, and Huntington's disease.[34] According to the literature, BSA protein exhibits irreversible aggregation in the presence of different kinds of electrolytes such as Na_2SO_4 and NaSCN, and nonelectrolytes such as sucrose, sorbitol, and urea.[21] Herein, for our fundamental understanding in connection with reversible aggregation, we have chosen ADA as a guest molecule as it has a higher binding affinity towards CB7.[35] When we added ADA into the turbid solution, astonishingly, it turned into a clear solution. The reversibility has been proved by the simultaneous addition of CB7 and ADA into the BSA-Au NC solution (Fig. 3f).

In conclusion, utilizing the supramolecular host–guest chemistry of CB7 in BSA-Au NCs, we design a higher-order assembled system which exhibits a 40% absolute fluorescence

quantum yield. Furthermore, in the presence of CB7, BSA-Au NCs possess a negative charge while Lys-Au NCs exhibit a positive charge. In addition to that, the assembled structure of BSA-Au NCs shows reversible aggregation and disaggregation in the presence of cucurbit[7]uril and adamantylamine respectively, which is one of the important aspects in the fundamental study of protein aggregation. We are optimistic that our findings will fuel the applications of supramolecular cage-mediated protein-protected gold nanoclusters not only in biology but also as an optoelectronic material in the future.

Author contributions

Anjan Maity has designed the project, performed all experiments, analyzed all the data, and written the manuscript. Atul kumar has measured the absolute fluorescence quantum yield.

Conflicts of interest

Anjan Maity declares absolutely no conflict of interest.

Acknowledgements

Anjan Maity is grateful to Prime Minister's Research Fellowship (PMRF), Ministry of Education, Government of India (Application No: PMRF-192002-375). The author is thankful to Materials Research Centre, Inorganic and Physical Chemistry Department, CeNSE Department, Biological Sciences Division of Indian Institute of Science, Bangalore. Thanks to Horiba IISc Technical Centre, Bangalore facility and H. C. Sudeeksha, T. R. E. Rakesh for helping to acquire the lifetime data. We also thank Soumen Pradhan for his help in getting LC-MS data (JNCASR, Bangalore – 560064). Thanks to Subinoy Rana for lab support (January, 2020–January, 2022).

Notes and references

1 I. Chakraborty and T. Pradeep, *Chem. Rev.*, 2017, **117**, 8208–8271.
2 C. P. Joshi, M. S. Bootharaju and O. M. Bakr, *J. Phys. Chem. Lett.*, 2015, **6**, 3023–3035.
3 C. Zeng, Y. Chen, G. Li and R. Jin, *Chem. Commun.*, 2013, **50**, 55–57.
4 M. S. Bootharaju, V. M. Burlakov, T. M. D. Besong, C. P. Joshi, L. G. Abdulhalim, D. M. Black, R. L. Whetten, A. Goriely and O. M. Bakr, *Chem. Mater.*, 2015, **27**, 4289–4297.
5 C. P. Joshi, M. S. Bootharaju, M. J. Alhilaly and O. M. Bakr, *J. Am. Chem. Soc.*, 2015, **137**, 11578–11581.
6 A. Nag, P. Chakraborty, M. Bodiuzzaman, T. Ahuja, S. Antharjanam and T. Pradeep, *Nanoscale*, 2018, **10**, 9851–9855.
7 P. Maity, H. Tsunoyama, M. Yamauchi, S. Xie and T. Tsukuda, *J. Am. Chem. Soc.*, 2011, **133**, 20123–20125.
8 Z. Wu and R. Jin, *Nano Lett.*, 2010, **10**, 2568–2573.
9 Y. Chen, T. Yang, H. Pan, Y. Yuan, L. Chen, M. Liu, K. Zhang, S. Zhang, P. Wu and J. Xu, *J. Am. Chem. Soc.*, 2014, **136**, 1686–1689.
10 D. Bain, S. Maity and A. Patra, *Chem. Commun.*, 2020, **56**, 9292–9295.
11 X. R. Song, N. Goswami, H. H. Yang and J. Xie, *Analyst*, 2016, **141**, 3126–3140.
12 H. Li, W. Zhu, A. Wan and L. Liu, *Analyst*, 2017, **142**, 567–581.
13 C. M. Hofmann, J. B. Essner, G. A. Baker and S. N. Baker, *Nanoscale*, 2014, **6**, 5425–5431.
14 P. Chakraborty, A. Nag, A. Chakraborty and T. Pradeep, *Acc. Chem. Res.*, 2019, **52**, 2–11.
15 Nonappa, J. S. Haataja, J. V. I. Timonen, S. Malola, P. Engelhardt, N. Houbenov, M. Lahtinen, H. Häkkinen and O. Ikkala, *Angew. Chem.*, 2017, **129**, 6573–6577.
16 A. Nag, P. Chakraborty, A. Thacharon, G. Paramasivam, B. Mondal, M. Bodiuzzaman and T. Pradeep, *J. Phys. Chem. C*, 2020, **124**, 22298–22303.
17 A. Mathew, G. Natarajan, L. Lehtovaara, H. Häkkinen, R. M. Kumar, V. Subramanian, A. Jaleel and T. Pradeep, *ACS Nano*, 2014, **8**, 139–152.
18 J. S. Mohanty, K. Chaudhari, C. Sudhakar and T. Pradeep, *J. Phys. Chem. C*, 2019, **123**, 51.
19 Z. Huang, M. Wang, Z. Guo, H. Wang, H. Dong and W. Yang, *ACS Omega*, 2018, **3**, 12763–12769.
20 Z. Lu and Y. Yin, *Chem. Soc. Rev.*, 2012, **41**, 6874–6887.
21 H. L. Bagger, L. H. Øgendal and P. Westh, *Biophys. Chem.*, 2007, **130**, 17–25.
22 J. Xie, Y. Zheng and J. Y. Ying, *J. Am. Chem. Soc.*, 2009, **131**, 888–889.
23 D. Bardelang, K. A. Udachin, D. M. Leek, J. C. Margeson, G. Chan, C. I. Ratcliffe and J. A. Ripmeester, *Cryst. Growth Des.*, 2011, **11**, 5598–5614.
24 M. A. H. Muhammed, P. K. Verma, S. K. Pal, A. Retnakumari, M. Koyakutty, S. Nair and T. Pradeep, *Chem. – Eur. J.*, 2010, **16**, 10103–10112.
25 J. W. Lee, H. H. L. Lee, Y. H. Ko, K. Kim and H. I. Kim, *J. Phys. Chem. B*, 2015, **119**, 4628–4636.
26 T. Jiang, G. Qu, J. Wang, X. Ma and H. Tian, *Chem. Sci.*, 2020, **11**, 3531–3537.
27 F. Chandra, K. Pal, S. Lathwal and A. L. Koner, *Mol. Biosyst.*, 2016, **12**, 2859–2866.
28 L. Shang, R. M. Dörlich, S. Brandholt, R. Schneider, V. Trouillet, M. Bruns, D. Gerthsen and G. U. Nienhaus, *Nanoscale*, 2011, **3**, 2009–2014.
29 S. Raut, R. Chib, S. Butler, J. Borejdo, Z. Gryczynski and I. Gryczynski, *Methods Appl. Fluoresc.*, 2014, **2**, 035004.
30 H. Wei, Z. Wang, L. Yang, S. Tian, C. Hou and Y. Lu, *Analyst*, 2010, **135**, 1406–1410.
31 N. Barooah, A. Kunwar, R. Khurana, A. C. Bhasikuttan and J. Mohanty, *Chem. – Asian J.*, 2017, **12**, 122–129.
32 M. Stenrup, E. Pieri, V. Ledentu and N. Ferré, *Phys. Chem. Chem. Phys.*, 2017, **19**, 14073–14084.
33 J. Mei, N. L. C. Leung, R. T. K. Kwok, J. W. Y. Lam and B. Z. Tang, *Chem. Rev.*, 2015, **115**, 11718–11940.
34 C. A. Ross and M. A. Poirier, *Nat. Med.*, 2004, **10**, S10–S17.
35 M. A. Alnajjar, W. M. Nau and A. Hennig, *Org. Biomol. Chem.*, 2021, **19**, 8521–8529.